BULLETIN OF MARINE SCIENCE, 38(1): 35–55, 1986

VERTICAL DISTRIBUTION OF FALLOUT RADIONUCLIDES IN ENEWETAK LAGOON SEDIMENTS: EFFECTS OF BURIAL AND BIOTURBATION ON THE RADIONUCLIDE INVENTORY

Gary M. McMurtry, Randi C. Schneider, Patrick L. Colin, Robert W. Buddemeier and Thomas H. Suchanek

ABSTRACT

The lagoon sediments off Runit Island at Enewetak Atoll contain elevated concentrations of fallout radionuclides from nuclear device testing in the 1950's. Contrary to previous assumptions about the lagoon sediment radionuclide distribution, we have found large concentrations of ^{60}Co, ^{137}Cs, ^{125}Sb, ^{155}Eu, ^{207}Bi, ^{238}Pu, $^{239+240}Pu$ and ^{241}Am at depth in sediment cores up to 2 m in length. Transuranic isotope distributions determined by alpha track autoradiography reveal concentrations within the topmost 40 cm of most cores, whereas the other radionuclides are concentrated deeper in the cores. In the two most heavily contaminated cores, radionuclide concentrations correlate with a distinct layer of fine-grained (<38 μm) carbonate that probably represents blast-pulverized reef and sediments from a nearby barge event. Over 90% of the radioactivity within this layer is in an iron-rich noncarbonate residue that contains magnetite formed from the condensation of metallic apparatus vaporized by the fireball. Associated pyrite has formed in situ from the alteration of magnetite under anoxic conditions. The sampling area is heavily colonized by several species of burrowing callianassid ghost shrimp (Crustacea: Thalassinidea), and some of the cores show evidence of burrowing into the radioactive layers. The burrowing activities of these shrimp facilitate radionuclide remobilization within the lagoon by advection of sediment and porewater during sorting and pumping and by oxidation of suboxic sediments at depth.

Enewetak Atoll in the northern Marshall Islands was the site of 43 nuclear weapons tests during the 1948–1958 testing period (U.S.A.E.C., 1973; U.S.D.O.E., 1982). As a result of the testing, several of the islands in the atoll and extensive areas of its lagoon floor were severely contaminated with fallout radionuclides. Prior to rehabitation, a comprehensive radiological survey of the environment was conducted in 1972 (U.S.A.E.C., 1973) and a radiological cleanup of the islands was completed in 1980 (Defense Nuclear Agency, 1981; U.S.D.O.E., 1982).

The sediments of the lagoon floor continue to be the largest repository of fallout radionuclides (U.S.A.E.C., 1973; U.S.D.O.E., 1982). The Enewetak radiological survey of 1972 extensively studied the surface sediments of the lagoon and found two major areas of contamination: the northeast lagoon floor extending southwest of Enjebi and a smaller area extending southwest of Runit (U.S.A.E.C., 1973) (Fig. 1). Although the burial of fallout radionuclides has been studied on the islands (Gudiksen and Lynch, 1975; Bliss, 1982; U.S.D.O.E., 1982) and in several of the large craters, (U.S.A.E.C., 1973; Ristvet, 1978) no study of their vertical distribution in the lagoon sediments has been conducted below a sediment depth of about 20 cm. Because these sediments contain a significant amount of the atoll radionuclide inventory and possess an active, burrowing infauna, we investigated the vertical distribution of fallout radionuclides in a series of cores taken by SCUBA divers within the contaminated area southwest of Runit Island (Fig. 2).

Runit Island (named Yvonne during the testing period) received the most severe radiological impact of any island within the atoll (Gudiksen and Lynch, 1975). Eight nuclear tests were conducted on the island and 10 additional tests were

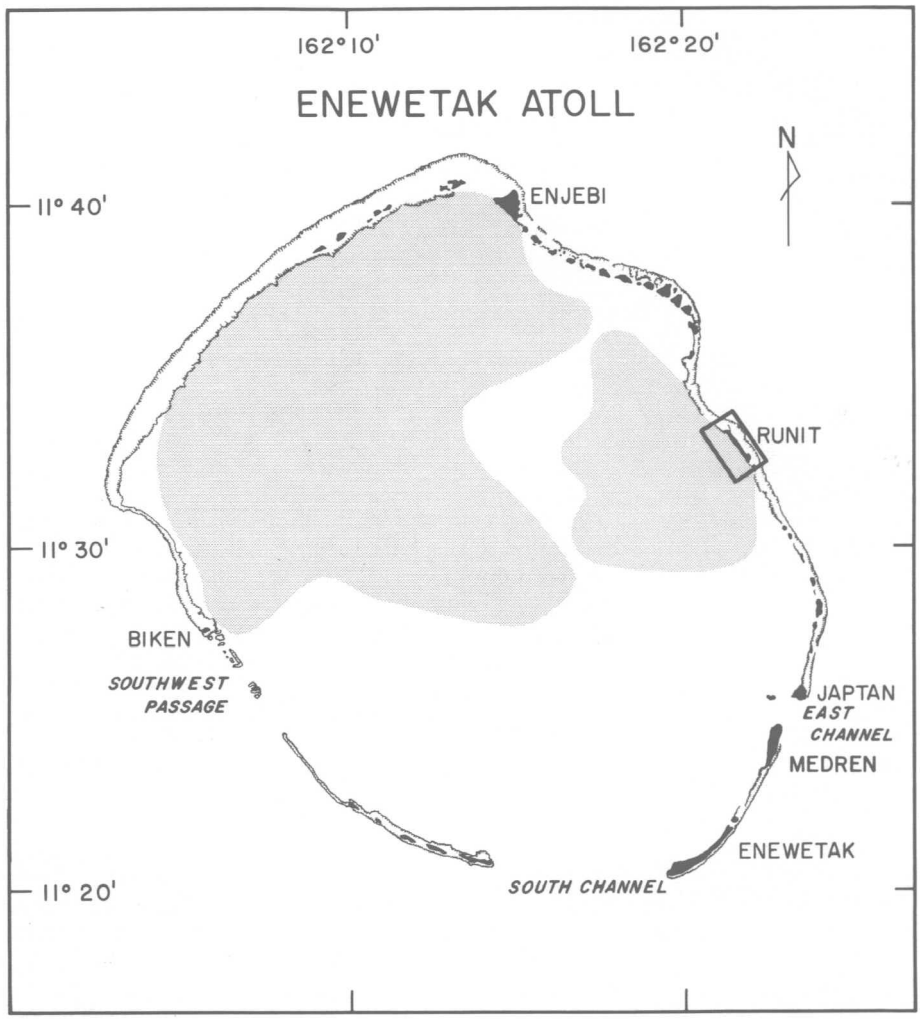

Figure 1. Location map of Enewetak Atoll, Marshall Islands. Shaded areas are lagoon sediments with greater than 100 mCi/km^2 $^{239+240}$Pu. Box indicates location of detailed study area off Runit (Fig. 2). Modified after U.S.A.E.C. (1973).

conducted (most on floating barges) in its vicinity (Table 1 and Fig. 2). Because of these tests, the area surrounding Runit was contaminated with a complex assemblage of fission and activation products, of which only the long-lived radionuclides and their decay products remain. ^{90}Sr, $^{239+240}$Pu, ^{137}Cs and ^{60}Co generally predominate among the long-lived radionuclides found in the island soil (Gudiksen and Lynch, 1975), whereas ^{90}Sr, $^{239+240}$Pu, ^{155}Eu, ^{241}Am, ^{207}Bi, ^{137}Cs, ^{60}Co, ^{125}Sb, ^{102m}Rh, ^{152}Eu, ^{101}Ru, ^{154}Eu, and ^{106}Ru are found in decreasing mean activity in the lagoon sediments (U.S.A.E.C., 1973).

The lagoon floor in the sampling area has patch reef, scattered *Halimeda* colonies and ubiquitous mounds of reworked sediment and associated sink holes produced by a population of several species of burrowing callianassid ghost shrimp (Crustacea: Thalassinidea). Callianassids sort massive quantities of sediment which are gleaned for organic material; burrow systems are known to extend to greater

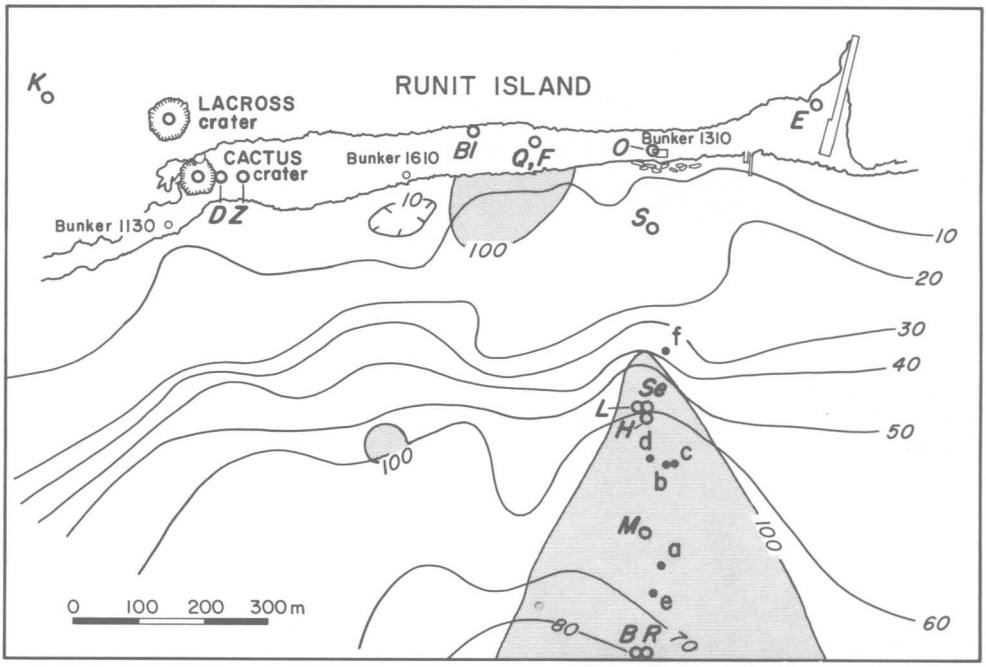

Figure 2. Detailed study area off Runit Island. Sample locations A through F and ground zero locations of various nuclear tests listed in Table 1 are indicated. Shaded areas are lagoon sediments with greater than 100 pCi/g $^{239+240}$Pu. Bathymetric contours in feet. Modified after U.S.A.E.C. (1973).

than 1.5 m below the sediment surface (Suchanek, 1983; Suchanek and Colin, this volume). Many of the cores described here were taken among dense calli-anassid mounds and some of them show evidence of burrowing at depth.

Methods

Eleven sediment cores ranging from 20 cm to 2 m in length were recovered in 40 to 70 feet of water (Fig. 2). SCUBA divers used 3-inch diameter plastic core liners that were hammered into the sediment, capped with plastic sheets and extracted. Sediment compression by these procedures was estimated visually to be about 20%. The cores were immediately frozen at the Mid-Pacific Research Laboratory (MPRL) at Enewetak and were later thawed, split lengthwise and stored under constant refrigeration at the Hawaii Institute of Geophysics (HIG) in Honolulu.

The sediment cores were initially surveyed for total gamma activity with a portable NaI (T1) detector at MPRL. After they were split at HIG, one core half was analyzed by gamma spectrometry and the other half by alpha and beta autoradiographic techniques.

The gamma spectrometer system used was specifically designed for core scanning (McMurtry, 1979; McMurtry et al., 1981). This system consists of a 3- by 3-inch flat-face NaI (T1) detector, Pb shielding and a Hewlett-Packard 5401A multichannel analyzer. The spectrometer was calibrated with known ^{60}Co, ^{137}Cs and ^{207}Bi solutions in sealed plastic containers designed to represent the geometry of the core halves. This calibration was checked with a known combination of the standard solutions analyzed under the same conditions as the core halves. Spectra were analyzed by the stripping technique (Ryback, 1971; Fankhauser, 1976; McMurtry, 1979).

Relative total alpha activities were determined by alpha track autoradiography (Fisher, 1977a; 1977b; Anderson and Macdougall, 1977; Buddemeier et al., 1978). Alpha-sensitive, Kodak LR-115 cellulose nitrate film was placed directly on the core and exposed for 1–2 months. Films were etched in a 10% NaOH solution at a constant temperature of 60°C. Etching efficiencies were monitored with a ^{241}Am source. Alpha tracks were counted by a random field of view method with a standard light microscope.

Table 1. List of events off Yvonne (Runit)*

Event	Date	Type and height (in feet) of burst	Lat. (N)	Long. (E)	Location/yield
Sandstone Series					
Zebra (Z)†	5/14/48	Tower, 200	11°33′21″	162°21′16″	Yvonne 18 KT
Greenhouse Series					
Dog (D)	4/7/51	Tower, 300	11°33′22″	162°21′16″	Yvonne
Ivy Series					
King (K)	11/16/52	Air, 1,480	11°33′42″	162°21′14″	1,800′ NW of Yvonne 500 KT
Red Wing Series					
Lacrosse	5/5/56	Surface + 17	11°33′29″	162°21′18″	Yvonne 40 KT Range
Erie (E)	5/30/56	Tower, 300	11°32′41″	162°21′52″	Yvonne
Blackfoot (Bl)	6/11/56	Tower, 200	11°33′04″	162°21′33″	Yvonne
Osage (O)	6/16/56	Air, 680	11°32′48″	162°21′39″	Yvonne
Hardtack Phase I Series					
Cactus	5/5/58	Surface + 3	11°33′23″	162°21′15″	Yvonne 18 KT
Butternut (B)	5/11/58	Barge + 10	11°32′28″	162°21′05″	4,000′ SW of Yvonne
Holly (H)	5/20/58	Barge + 13	11°32′38″	162°21′22″	2,075′ SW of Yvonne
Magnolia (M)	5/26/58	Barge + 14	11°32′34″	162°21′14″	3,000′ SW of Yvonne
Rose (R)	6/2/58	Barge + 15	11°32′28″	162°21′05″	4,000′ SW of Yvonne
Linden (L)	6/18/58	Barge + 8	11°32′39″	162°21′23″	2,000′ SW of Yvonne
Sequoia (Se)	7/1/58	Barge	11°32′39″	162°21′22″	2,000′ SW of Yvonne
Scaevola (S)	7/14/58	Barge + 20	11°32′46″	162°21′35″	560′ SW of Yvonne
Pisonia	7/18/58	Barge + 6.5	11°32′52″	162°19′39″	12,000′ W of Yvonne
Quince (Q)	8/6/58	Surface + 3	11°32′59″	162°21′34″	Yvonne
Fig (F)	8/14/58	Surface + 1.5	11°32′59″	162°21′34″	Yvonne

* Data after U.S. Dept. of Energy (1982) and B. Ristvet (pers. comm., 1982).
† Abbreviations in parentheses correspond to notations on Figure 2.

Relative total beta activities were assessed by a method similar to that described in Knutson et al. (1972). Kodak AA-2 Industrial X-ray film was placed on the core for 2 to 4 months. A 0.5-mil-thick plastic sheet was placed between the core and X-ray film to help prevent chemical reactions and alpha particle exposure. Developed films were analyzed by densitometry. The results of these procedures are presented elsewhere (McMurtry et al., 1985).

Subsamples of the cores were rinsed in distilled, deionized water and size fractioned by wet sieving. The <38 μm fractions of 5C-1, 48–53 cm and 5D-3, 61.5 to 66.5 cm were singled out for further analytical work because they contained large amounts of radioactivity. These samples were treated with a sodium acetate-acetic acid buffer solution (SAAB) (pH 5.0) to remove carbonate phases (Jackson, 1974). Both carbonate and noncarbonate phases were chemically analyzed by atomic absorption spectrophotometry. These phases were also analyzed by X-ray diffractometry and by scanning electron microscopy with energy-dispersive X-ray analysis (SEM/EDAX).

The size fractions and carbonate and noncarbonate fractions of 5C-1 and 5D-3 were assayed for gross alpha plus beta activity by liquid scintillation counting. Splits of some of these fractions were analyzed by gamma spectrometry and by alpha track autoradiography. Sediment samples were acidified with concentrated HCl and diluted with Aquasol® prior to liquid scintillation counting with a Beckman LS-100 counter. Reported gross activities are the summation of net cpm in standard energy windows (^{3}H, ^{14}C, ^{32}P). Rinse waters and SAAB solutions were concentrated by evaporation prior to gamma spectrometry. These solutions, the size fractions and the noncarbonate residues of 5C-1 and 5D-3 were sealed in plastic petri dishes and placed directly beneath the NaI (Tl) detector of the gamma spectrometer. The spectrometer was calibrated and checked with known ^{60}Co, ^{137}Cs and ^{207}Bi solutions in the same geometry as the petri dish samples.

Results

The lagoon sediments are primarily composed of an unconsolidated mixture of the skeletal remains of corals, coralline algae (*Halimeda* spp.) and foraminifera

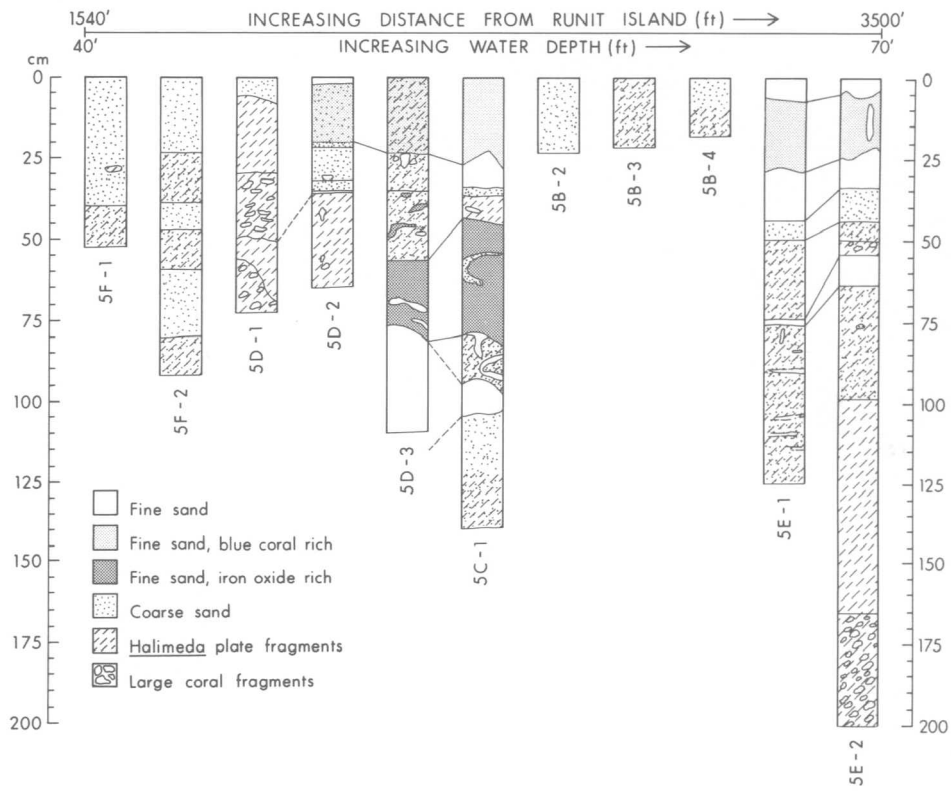

Figure 3. General lithologic descriptions of sediment cores.

(Emery et al., 1954). Major lithologic units of the sediment cores are schematically represented in Figure 3. Although the lagoon floor in the sampling area is heavily populated by callianassids, evidence of extensive bioturbation is apparent in only two of the cores (5C-1 and 5D-3) (Fig. 3 and Suchanek et al., this volume). Layering is evident in most of the cores, and one core (5E-2) appears to have graded bedding (Fig. 3).

Despite the relatively close spacing of the sampling sites (Fig. 2), only two layers can be identified with any degree of confidence in more than one core. These are the iron-rich silt and the "blue coral"-rich fine sand (Fig. 3). (The blue coral in these sediments is only tentatively identified; the grains appear to be coated with a blue layer.) Both layers are correlated with increased radioactivity (Fig. 4).

Detailed vertical distributions of total alpha activity and ^{60}Co, ^{137}Cs and ^{207}Bi activity are presented in Figure 4. The total alpha activity is representative of the transuranic radionuclides in these sediments, specifically ^{238}Pu, $^{239+240}Pu$, and ^{241}Am (Buddemeier et al., 1978) and are generally correlated with the measured activities of these isotopes in selected sections of the sediment cores (McMurtry et al., 1985). ^{60}Co, ^{137}Cs and ^{207}Bi are among several long-lived radionuclides that predominate in these sediments (Table 2).

Total alpha activities are presented as the mean alpha track production density per 6 cm of core in tracks/cm^2 min. Mean track densities peak in most cores in the topmost 40 cm and are generally not well correlated spacially or in magnitude with the ^{60}Co, ^{137}Cs or ^{207}Bi distributions (Fig. 4). Alpha track densities show

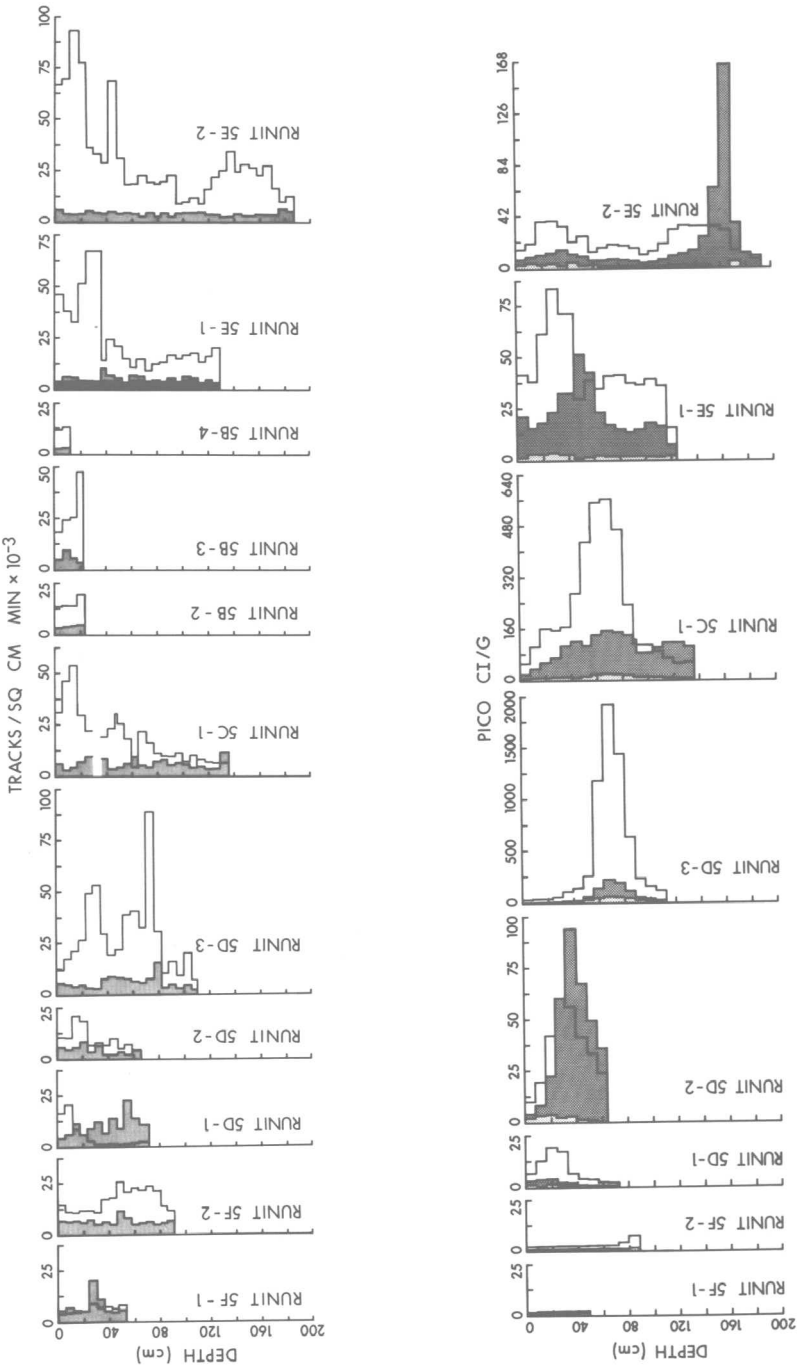

Figure 4. Detailed activity profiles. Top: Total alpha activity in tracks/cm² min × 10^{-3}. Shaded values are coefficient of variation × 10^{-1}. Bottom: ^{60}Co, ^{137}Cs and ^{207}Bi activities in pCi/g.

Table 2. Selected radionuclide concentrations in the vicinity of Runit (pCi/g)*

Ident.	^{60}Co	^{90}Sr	^{125}Sb	^{137}Cs	^{155}Eu	^{207}Bi	^{238}Pu	$^{239+240}$Pu	^{241}Am
Southern† Runit soil	0.01–20 (0.64)	0.09–20 (1.7)	—	0.02–3.6 (0.40)	—	—	—	0.02–50 (3.2)	—
Northern† beaches	0.03–1.6 (0.13)	1.2–30 (6.4)	—	0.03–9.0 (0.30)	—	—	—	0.34–18 (2.7)	—
Lagoon‡ surface	0.19–18 (1.6)	—	—	—	0.82–54 (5.5)	0.17–7.9 (0.47)	1.1–96 (6.2)	3.1–190 (26)	0.09–31 (2.2)
Lagoon§ cores	39–4,662 (180)	—	4.8–1,420 (33)	2.3–204 (15)	46–1,447 (132)	0.12–4.4 (0.58)	0.75–39 (8.2)	8.1–360 (82)	1.2–56 (12)

* The activities approximate log-normal distributions. Values reported are range and geometric mean (bracketed).
† From 51 surface (0–15 cm) samples randomly selected during 1972 survey (Gudiksen and Lynch, 1975).
‡ From 59–66 samples collected during 1972 survey in same area as shown in Figure 2 (U.S.A.E.C., 1973).
§ From 10 samples of cores 5C-1 and 5D-3 collected in 1981 (McMurtry et al., 1985), decay-corrected to 1972 for comparison.

some correlation with a layer of blue coral-rich fine sand identified in the most heavily contaminated cores (Figs. 3 and 4).

The coefficient of variation of the track densities (standard deviation/mean $\times 10^2$) is also shown in Figure 4 (shaded). The coefficient was calculated from thirty random fields of view per 6 cm of film and gives a measure of relative track density uniformity. This value increases where track density clusters characteristic of particulate-associated transuranics (Buddemeier et al., 1978) are encountered. The coefficient of variation generally increases in the cores nearest Runit, suggesting a relative increase in transuranic heterogeneity with decreasing distance from the island.

The vertical distributions of ^{60}Co, ^{137}Cs and ^{207}Bi display activity peaks at various depths throughout the cores (Fig. 4). Only in the two cores with the highest concentrations of these radionuclides are these peaks associated with a well-defined lithologic unit (5C-1 and 5D-3). This unit is predominately composed of fine-grained (<38 μm) carbonate that probably represents blast-pulverized sediment and reef material formed by cratering of nearby barge events. Similar fine-grained sediments have been observed in and adjacent to the Enewetak nuclear craters on land (Ristvet, 1978). The iron-rich nature of this sediment is discussed below.

The distributions of ^{60}Co, ^{137}Cs and ^{207}Bi correlate well with themselves and with the fine-grained carbonate layer only in core 5D-3, which also contains the largest concentrations of these radionuclides. These correlations decrease in core 5C-1, which appears to be more heavily bioturbated, and in the surrounding sediments (Fig. 4). If we assume a simultaneous fallout input from the various barge events, these distributions suggest differential mobilities of the transuranics, ^{60}Co, ^{137}Cs and ^{207}Bi in these sediments.

To better understand the activity distributions, cores 5C-1 and 5D-3 were singled out for more detailed work. Three samples were taken from each core: one from the surface, one in, and one below the highly radioactive, fine-grained carbonate layers. These samples were sized into seven fractions: >500, 246–500, 147–246, 74–147, 43–74, 38–43 and <38 μm. Each fraction was weighed and analyzed for gross alpha plus beta activity, total alpha activity and, in the fine-grained carbonate samples, for ^{60}Co, ^{137}Cs and ^{207}Bi activity. The results of these analyses are presented in Tables 3, 4 and 5 and in Figures 5 and 6.

Approximately 80% of the sediment mass is finer than 48 μm in the highly radioactive layers of 5C-1 and 5D-3, whereas coarser material predominates in the sediments above and below these layers. Although the <48-μm fractions contain large amounts of radioactivity, the coarser fractions apparently also contain significant amounts. This is especially so in the 147–246-μm fraction of 5D-3, 61.5–66.5 cm (Fig. 5). The large amounts of radioactivity in the coarser fractions could be a result of incomplete sizing of highly radioactive, fine-grained material that adheres to the rough surfaces of larger grains. Incomplete sizing is likely to occur but the extent of such fine particle adherence in the wet sieving procedures is unknown. Further, in the 147–246-μm fraction of 5D-3 the amount of radioactivity generally exceeds that of the finest, <38-μm fraction (Tables 3–5, Fig. 5).

To further investigate this anomalous situation, an adjacent sample of core 5D-3, 61.5–66.5 cm was analyzed. Sizing resulted in significantly different mass and radioactivity distributions but with total activities that are generally within the counting error (Tables 4 and 5, Fig. 6). The greater amounts of coarse-grained material in the original sample were traced to a burrow, possibly of a callianassid, which was inadvertently sampled. The large amounts of radioactivity in the 147–246-μm fraction of the original sample may be the result of bioaccumulation

Table 3. Size distribution of gross alpha plus beta activity in Runit cores (cpm/g)*

Core	Depth (cm)	Grain size (μm)							
		>500	500–246	246–147	147–74	74–43	43–38	<38	Total
5C-1	0–5	910 (2.6)	1,110 (2.8)	990 (7.6)	990 (32.3)	720 (37.0)	890 (3.6)	2,060 (14.0)	1,040
	48–53	1,930 (2.2)	1,810 (1.1)	1,490 (2.1)	1,920 (4.4)	1,880 (5.7)	3,210 (11.4)	3,880 (73.1)	3,490
	133–138	1,020 (11.0)	790 (9.8)	720 (24.4)	650 (31.0)	510 (13.1)	1,630 (2.3)	2,500 (8.3)	880
5D-3	0–5	440 (27.7)	430 (3.8)	620 (7.6)	500 (18.1)	330 (24.1)	570 (5.6)	1,530 (13.1)	590
	61.5–66.5	3,920 (1.5)	6,900 (0.7)	11,700 (1.9)	5,470 (2.6)	3,020 (11.9)	7,770 (46.9)	10,100 (34.4)	7,950
	109–113	910 (4.5)	710 (3.3)	460 (20.6)	390 (49.5)	320 (15.5)	760 (2.6)	2,370 (4.0)	520

* Activities determined by liquid scintillation counting of totally dissolved samples. Errors, based on counting statistics ($\pm 1\sigma$), are 2% of the reported values. Values in parentheses are the relative amounts of sample in each size fraction by weight percent.

Table 4. Size distribution of total alpha activity in Runit cores (tracks/cm^2 min $\times 10^{-3}$)

Core	Depth (cm)	Grain size (μm)							
		>500	500–246	246–147	147–74	74–43	43–38	<38	Total†
5C-1	0–5	31 ± 1	22 ± 1	47 ± 2	72 ± 2	49 ± 2	50 ± 2	94 ± 3	61 ± 5
	48–53	44 ± 2	28 ± 1	32 ± 1	51 ± 1	58 ± 2	89 ± 4	76 ± 2	73 ± 6
	133–138	10 ± 1	8 ± 1	6 ± 1	6 ± 1	7 ± 1	12 ± 1	30 ± 2	9 ± 3
5D-3	0–5	64 ± 2	73 ± 2	76 ± 2	57 ± 2	46 ± 2	65 ± 2	133 ± 4	69 ± 6
	61.5–66.5	96 ± 4	34 ± 3	610 ± 20	240 ± 10	119 ± 3	310 ± 10	390 ± 10	310 ± 30
	61.5–66.5*	—	—	128 ± 7	72 ± 2	143 ± 3	91 ± 3	338 ± 5	320 ± 10
	109–113	17 ± 1	16 ± 1	10 ± 1	8 ± 1	7 ± 1	12 ± 1	43 ± 2	10 ± 3

* Adjacent sample of core.
† Total activity based on weight fraction percentages in Tables 3 and 5.

Table 5. Size distribution of ^{60}Co, ^{137}Cs and ^{207}Bi activity in Runit cores*

Sample ident.	Grain size (μm)	Weight fraction (%)	^{60}Co (pCi/g)	^{137}Cs (pCi/g)	^{207}Bi (pCi/g)	$^{137}Cs/^{60}Co$	$^{207}Bi/^{60}Co$
5C-1	>500	2.2	110 ± 3	50 ± 3	12 ± 2	0.45 ± 0.03	0.110 ± 0.020
48–53 cm	500–246	1.1	101 ± 5	35 ± 5	0 ± 5	0.35 ± 0.05	0.000
	246–147	2.1	90 ± 2	35 ± 2	7 ± 2	0.39 ± 0.02	0.070 ± 0.020
	147–74	4.4	130 ± 5	44 ± 1	5 ± 1	0.34 ± 0.02	0.040 ± 0.010
	74–43	5.7	180 ± 10	50 ± 2	5 ± 1	0.29 ± 0.02	0.030 ± 0.010
	43–38	11.4	350 ± 10	71 ± 3	7 ± 1	0.20 ± 0.01	0.020 ± 0.003
	<38	73.1	620 ± 25	115 ± 5	9 ± 1	0.19 ± 0.01	0.015 ± 0.002
5D-3	>500	1.5	640 ± 20	73 ± 6	0 ± 5	0.11 ± 0.01	0.000
61.5–66.5 cm	500–246	0.7	1,250 ± 40	100 ± 20	0 ± 10	0.08 ± 0.02	0.000
	246–147	1.9	2,220 ± 90	250 ± 10	18 ± 3	0.11 ± 0.01	0.008 ± 0.002
	147–74	2.6	720 ± 30	80 ± 2	2 ± 2	0.11 ± 0.01	0.003 ± 0.003
	74–43	11.9	450 ± 20	33 ± 1	2 ± 1	0.07 ± 0.01	0.004 ± 0.002
	43–38	46.9	1,310 ± 50	139 ± 6	16 ± 1	0.11 ± 0.01	0.012 ± 0.001
	<38	34.4	2,180 ± 90	230 ± 10	16 ± 1	0.11 ± 0.01	0.007 ± 0.001
5D-3†	>500	—	—	—	—	—	—
61.5–66.5 cm	500–246	—	—	—	—	—	—
	246–147	0.4	103 ± 8	30 ± 8	15 ± 5	0.29 ± 0.08	0.140 ± 0.050
	147–74	0.5	600 ± 20	34 ± 6	11 ± 4	0.06 ± 0.01	0.020 ± 0.010
	74–43	3.9	290 ± 10	14 ± 1	4 ± 1	0.05 ± 0.01	0.014 ± 0.003
	43–38	2.0	188 ± 7	19 ± 2	3 ± 1	0.10 ± 0.01	0.020 ± 0.010
	<38	93.2	1,600 ± 65	214 ± 9	44 ± 2	0.13 ± 0.01	0.028 ± 0.002

* Analyses by gamma spectrometry using a NaI (Tl) detector. Errors based on counting statistics ($\pm 1\sigma$).
† Adjacent sample of core.

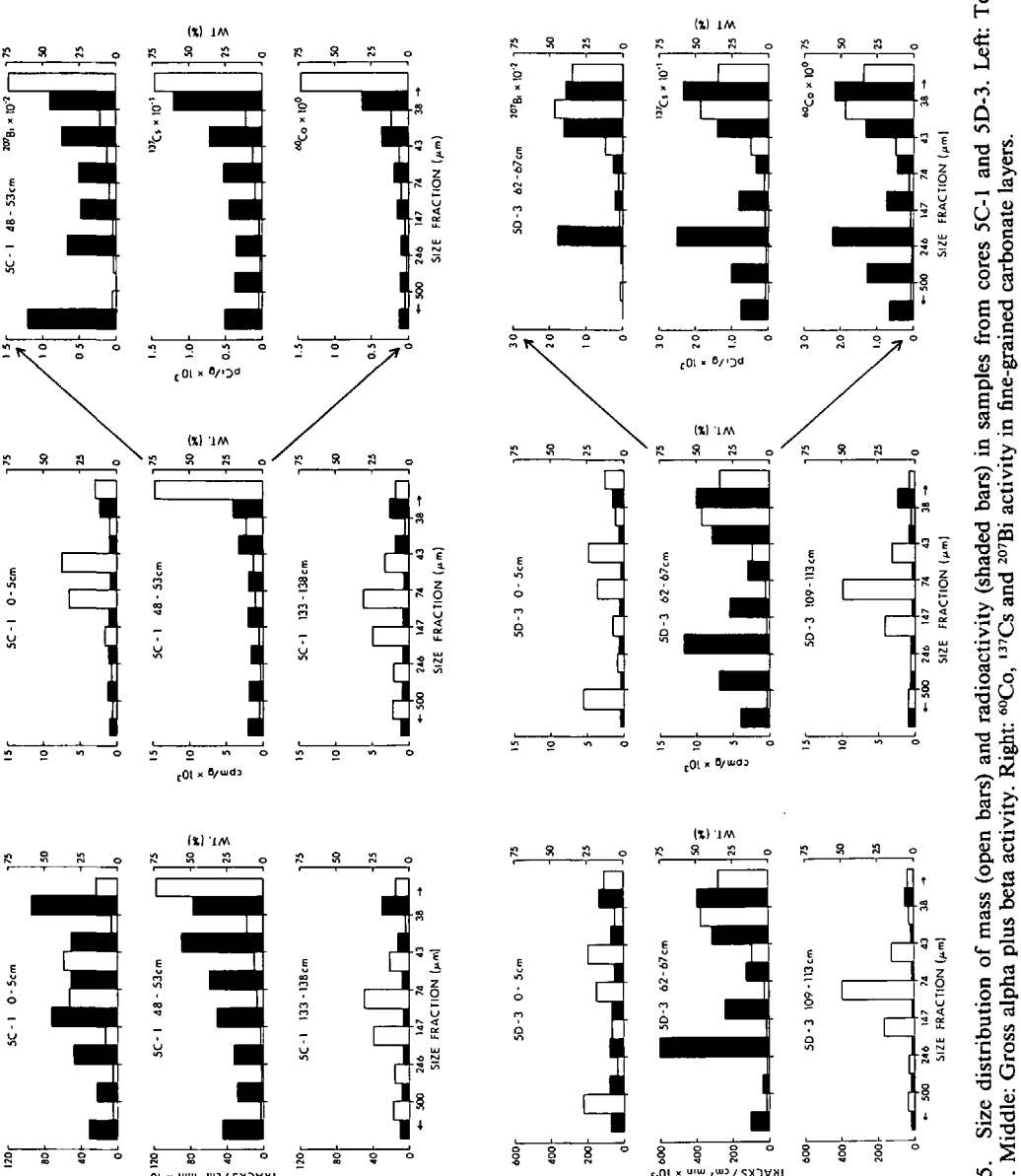

Figure 5. Size distribution of mass (open bars) and radioactivity (shaded bars) in samples from cores 5C-1 and 5D-3. Left: Total alpha activity. Middle: Gross alpha plus beta activity. Right: ^{60}Co, ^{137}Cs and ^{207}Bi activity in fine-grained carbonate layers.

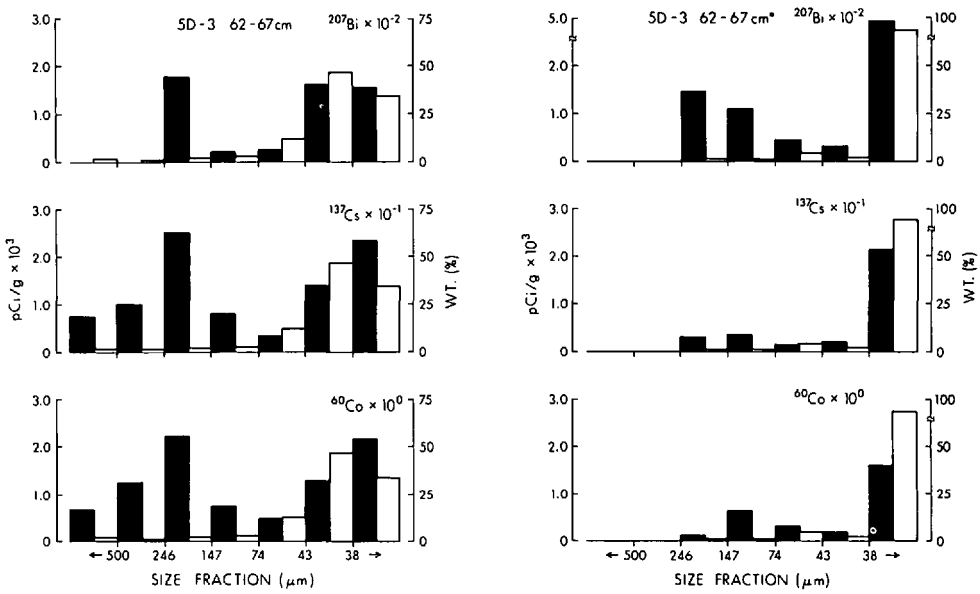

Figure 6. Comparison of mass (open bars) and radioactivity (shaded bars) size distribution in two adjacent samples of the fine-grained carbonate layer in core 5D-3. The sample on the left contained a callianassid burrow.

(Davis and Foster, 1958), possibly in the mucus lining of the burrow. Further work will be necessary to resolve the exact origins of this radioactivity distribution.

Examination of the mass and radioactivity distributions from the adjacent sample of the 5D-3 fine-grained carbonate layer and from that of the 5C-1 fine-grained carbonate layer indicate that normally most of the mass and radioactivity in these layers resides in the <38-μm fraction. Visual inspection of the cores both immediately after retrieval and after splitting revealed black and greyish-brown colors, respectively, for the fine-grained carbonate layers of 5D-3 and 5C-1. This suggested the presence of additional phases that bulk chemical analyses indicated were iron-rich. Carbonate dissolution of the <38-μm fraction of the fine-grained carbonate samples was undertaken to isolate and identify the additional phases and to determine the distribution of radioactivity between these phases and the carbonate.

X-ray mineralogy studies of the carbonate dissolution residues reveal that the noncarbonate material consists largely of magnetite with minor amounts of pyrite. Trace quantities of quartz, plagioclase and smectite of probable aeolian origin are also present (Fig. 7). SEM/EDAX studies (Figs. 8 and 9) indicate minor amounts of amorphous biogenic silica and reveal that the pyrite has formed in situ by postdepositional interaction of the magnetite and porewater sulfate under anoxic conditions.

Adams et al. (1960) found that fallout particles collected following nuclear detonations at Enewetak had formed by the interaction of condensing vaporized metals and fission products from the bomb and associated structures with surface material swept up into the cooling fireball. In the case of barge events, most of these particles were small (<1 μm) spheres of dicalcium ferrite formed from the condensation of the vaporized barge and ballast materials. Adams et al. (1960)

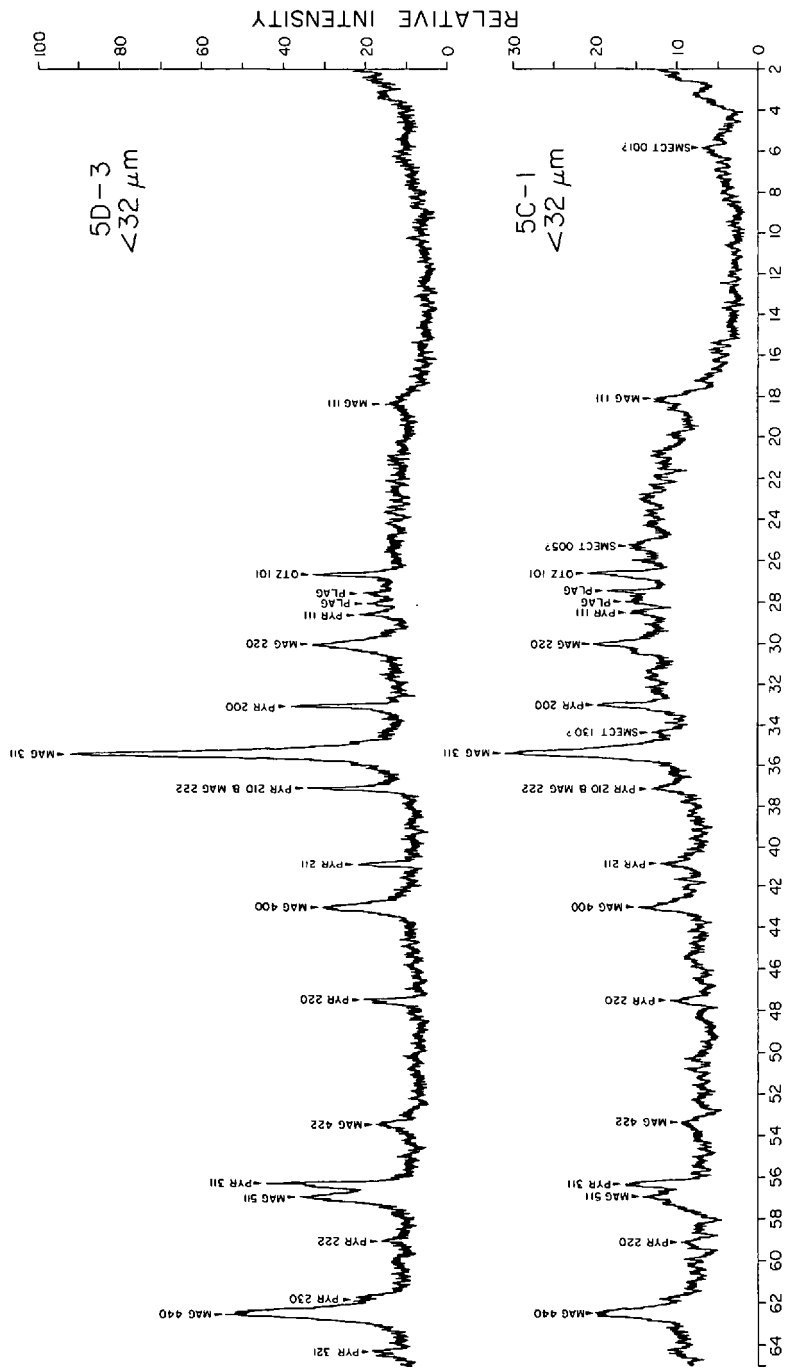

Figure 7. X-ray diffraction patterns of the SAAB nonextractable fractions of 5C-1, 48–53 cm, <38 μm and 5D-3, 61.5–66.5 cm, <38 μm. Oriented mounts on glass slides. CuK_α radiation. Scan rates at 2° 2θ/min.

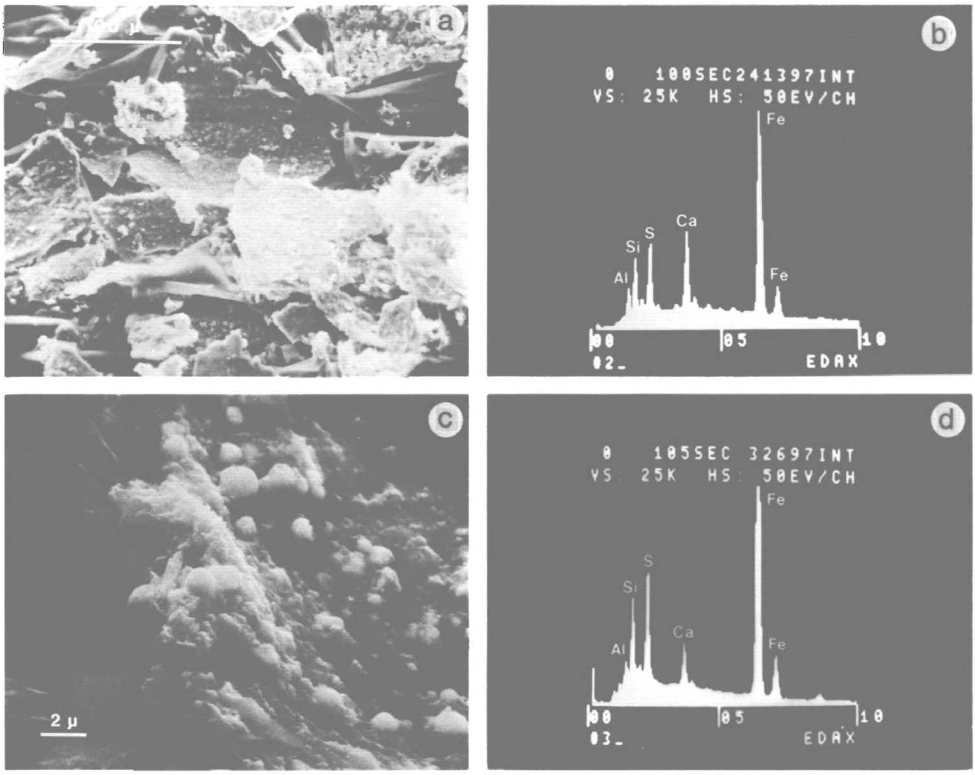

Figure 8. Scanning electron micrographs and corresponding EDAX spectrums of the SAAB nonextractable fractions of (a) and (b) 5C-1 and (c) and (d) 5D-3. Note platy habit (a) and scattered pyrite "spheres" on plate (c and Fig. 9). (b) and (d) are low magnification (300×) energy dispersive X-ray spectrums.

identified magnetite and calcium oxide as major components of fallout particles from tower and ground shots on land.

The noncarbonate material of these layers contains greater than 90% of the gross alpha plus beta activity. The partitioning of ^{60}Co, ^{137}Cs, ^{207}Bi and total alpha activity in the <38-μm fraction of the 5C-1 and 5D-3 fine-grained carbonate layers is presented in Table 6. ^{60}Co activity is highly concentrated in the SAAB nonextractable or noncarbonate material, whereas ^{207}Bi and ^{137}Cs activities display increasing partitioning into the water soluble and SAAB extractable (carbonate) fractions. Total alpha activities show the largest partitioning into the SAAB solution. Although we could not reliably measure the transuranic activity in the water soluble fraction because of the nature of the total alpha measurements, the measurements suggest that transuranics are more widely distributed than ^{60}Co in these sediments (Table 6).

Discussion

Probably most of the radioactivity in the fine-grained carbonate layers of 5C-1 and 5D-3 was originally present in the magnetite. Subsequent to what was probably a nearly instantaneous deposition of the fine-grained carbonate layer, deposition

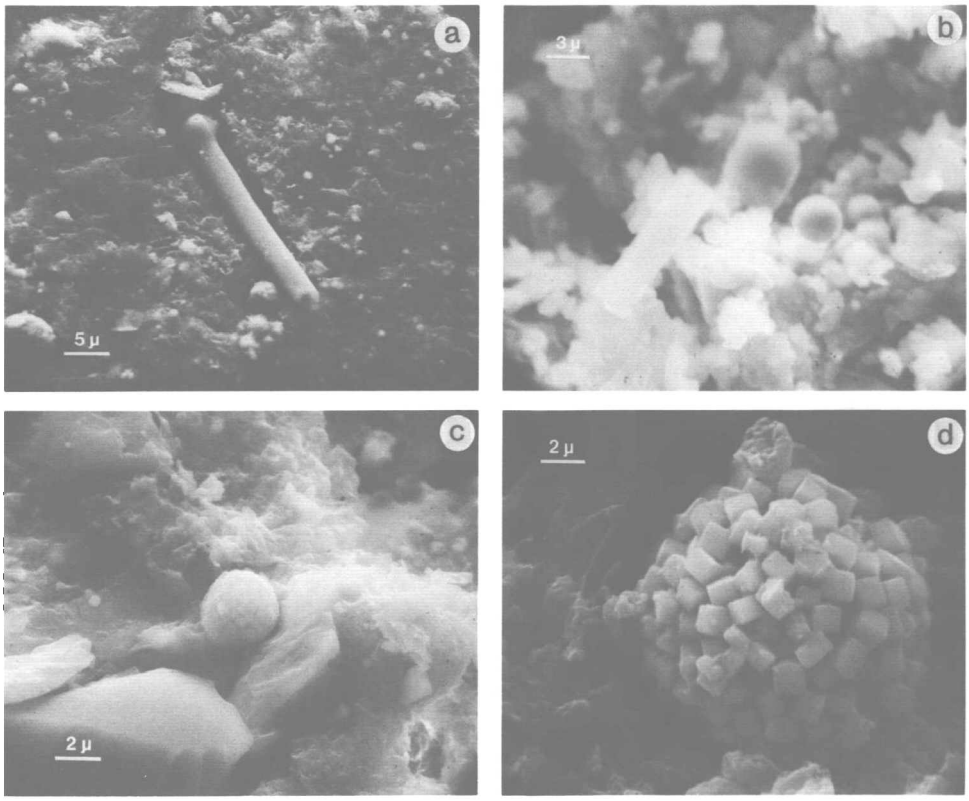

Figure 9. Scanning electron micrographs of the SAAB nonextractable fractions of 5C-1 and 5D-3. (a) Broken sponge spicule in 5D-3; (b) a small sphere of unknown origin in 5C-1 primarily composed of Ca, Al and Si (right of center); (c) close-up of small pyrite "sphere" in 5D-3 (center); (d) a large pyrite "sphere" in 5D-3 showing radiating cube habit. These delicate growth features indicate an in situ origin for the pyrite.

of predominately coarser-grained sediments occurred by either slumping or normal sedimentation, or some combination of these processes. Average sedimentation rates since 1958 at these two core sites derived from the top of the fine-grained carbonate layers are 1.9 and 2.4 cm/year, respectively. These averages should be viewed with caution because of: (1) the likelihood of slumping due to adjacent blasts or subsequent downslope movements, and (2) the bioturbation.

After burial, anoxia and bioturbation have caused the redistribution of some of the radioactivity originally absorbed into the magnetite. The presence of secondary pyrite indicates that anoxic conditions have remobilized some of the iron in solution to react with porewater sulfide, a reaction primarily controlled by the availability of organic matter that can be metabolized by sulfate-reducing bacteria (Berner, 1970). The differential mobility and upward migration of plutonium in the sediment column relative to ^{137}Cs has been suggested to be caused by anoxic conditions at depth (Livingston and Bowen, 1979). The relative activity profiles of the lagoon cores suggest some mobility and upward migration of transuranics

Table 6. Partitioning of ^{60}Co, ^{137}Cs, ^{207}Bi and total alpha activity in Runit cores

Sample ident.	Radionuclide*	Water soluble†	%	SAAB extractable	%	SAAB nonextractable	%	Total activity§	
								Calculated	Measured
5C-1	^{60}Co	0.32 ± 0.05	0.1	133 ± 5	0.5	27,000 ± 1,000	99.4	460 ± 10	620 ± 25
48–53 cm	^{137}Cs	18.1 ± 0.8	15.5	61 ± 3	1.4	3,500 ± 100	83.1	102 ± 3	115 ± 5
<38 μm	^{207}Bi	0.63 ± 0.03	7.1	7.7 ± 0.4	2.0	360 ± 20	90.9	12 ± 1	9 ± 1
	Total alpha	—	—	60 ± 2‡	3.3	1,730 ± 50	96.7	—	76 ± 2
5D-3	^{60}Co	0.89 ± 0.07	0.1	390 ± 10	0.7	56,000 ± 2,000	99.2	1,560 ± 40	1,600 ± 65
61.5–66.5 cm	^{137}Cs	14.0 ± 0.7	6.5	83 ± 3	1.2	6,400 ± 300	92.3	216 ± 7	214 ± 9
<38 μm	^{207}Bi	0.83 ± 0.04	2.0	7.0 ± 0.8	0.6	1,170 ± 30	97.4	31 ± 1	44 ± 2
	Total alpha	—	—	270 ± 5‡	7.1	3,520 ± 50	92.9	—	338 ± 5

* ^{60}Co, ^{137}Cs and ^{207}Bi activities in pCi/g; total alpha activities in tracks/cm^2 min × 10^{-3}. Errors based on counting statistics.
† Activities and percentages based on distilled/deionized water rinse of bulk sample. Other percentages adjusted to reflect rinse loss.
‡ Calculated from difference of total and SAAB nonextractable activities on the basis that nonextractables account for 1.2 and 2.1% of 5C-1 and 5D-3 samples, respectively.
§ Total activity after rinsing calculated by summation of weighted SAAB extractable and nonextractable activities.

relative to ^{60}Co, ^{137}Cs and ^{207}Bi (Fig. 4). Such transuranic mobility, however, is not supported by laboratory or field studies (Alberts and Orlandini, 1981; Carpenter and Beasley, 1981; Santschi et al., 1983) or by the partitioning results presented here (Table 6). The total alpha activity profiles more likely reflect a complex transuranic deposition pattern in this area of the lagoon.

Of the two cores that readily display the effects of callianassid bioturbation, core 5C-1 appears to be more heavily bioturbated than 5D-3. These two cores, which were located within 60 m of one another, also contain the lithologically similar, iron-rich, fine-grained carbonate layer. The similar chemistry, mineralogy and radionuclide composition of these layers suggest that they contain fallout from the same or similar nuclear events—probably either Holly, Linden or Sequoia (Fig. 2).

The fine-grained carbonate layer of core 5C-1 contains only one third to one half of the radioactivity and iron content of core 5D-3 (Tables 3–6). Disregarding the 5D-3 sample containing a burrow, the 5C-1 layer has more coarse-grained material than the 5D-3 layer. These observations are consistent with either greater mixing of less radioactive material into or greater transport of radioactive material out of the 5C-1 fine carbonate layer by callianassid burrowing.

The relative distributions of ^{60}Co and ^{137}Cs activity in both cores suggest that ^{137}Cs is more mobile than ^{60}Co in core 5C-1 (Fig. 4). Model ecosystem and coastal marine sediment studies have shown that ^{137}Cs transport is controlled by molecular diffusion through sediment pore waters, and that this transport is enhanced by bioturbation (Santschi et al., 1983). The relative ^{137}Cs distribution in the two cores and the twofold increase in water soluble ^{137}Cs measured in the 5C-1 fine carbonate layer over that of 5D-3 (Table 6) support bioturbation enhancement of ^{137}Cs mobility, although the specific mechanisms for such mobilization are not clear. Bioturbation clearly redistributes particulate phases and, together with pore water advection by callianassid burrowing and pumping, certainly enhances the mobility of relatively soluble radionuclides such as ^{137}Cs. Transport in the dissolved state, however, must first involve release of radionuclides absorbed into the fallout particles.

Oxidation of the magnetite and pyrite by relatively oxygenated pore waters introduced by callianassids is one potential mechanism for radionuclide release suggested by our observations. Black and greyish-brown colors exhibited by the fine-grained carbonate layers of the cores both immediately after retrieval and after splitting indicated the relative oxidation of 5C-1. Although the noncarbonate fractions of both fine carbonate layers contain similar amounts of iron (Table 7 and Fig. 8), the X-ray mineralogy results (Fig. 7) indicate that the noncarbonate fraction of 5C-1 contains only about a third of the magnetite and pyrite of 5D-3 but contains substantially more X-ray amorphous material. This material may be amorphous ferric oxide formed as an oxidation product. The greater percentage of water soluble ^{137}Cs and ^{207}Bi activity and the generally twofold-lower specific activity of the 5C-1 noncarbonate fraction (Table 6) are possibly a consequence of magnetite and pyrite oxidation. These reactions can be represented as:

$$2Fe_3O_4 + 0.5O_2 \rightarrow Fe_2O_3 \qquad \text{(magnetite)} \qquad (1)$$

$$2FeS_2 + 7.5O_2 + 4H_2O \rightarrow Fe_2O_3 + 8H^+ + 4SO_4^{2-} \qquad \text{(pyrite)} \qquad (2)$$

Sulfuric acid formed by the hydrolysis of the pyrite oxidation products (eq. 2) may further enhance the release of radionuclides in these sediments by lowering porewater pH in the vicinity of the iron phases.

We have concentrated our efforts on cores 5C-1 and 5D-3 because both con-

Table 7. Chemical composition of SAAB nonextractable fraction*

Sample ident.	Element (wt. %)			
	Fe	Si	Al	Ca
5C-1, 48–53 cm <38 μm	9.5	8.8	2.4	1.8
5D-3, 61.5–66.5 cm <38 μm	8.0	15.1	2.5	0.51

* Partial chemical analyses by atomic absorption spectrophotometry. Both samples apparently contained organic residues which resisted concentrated HCl, HNO_3 and HF but reacted with 30% H_2O_2 and 70% perchloric acid solutions.

tained large amounts of radioactivity associated primarily with a well-defined lithologic unit and because they readily displayed varying amounts of bioturbation. The surrounding cores show no evidence of such a well-defined layer or, surprisingly, of bioturbation. Although further work is needed, we suspect that much of the radioactivity in these surrounding cores correlates with fine-grained carbonate material, similar to that of 5C-1 and 5D-3, which is dispersed in coarser-grained carbonate. The lower radioactivity of cores 5D-1, 5D-2, 5F-1 and 5F-2 generally supports such dispersion, but cores 5E-1 and 5E-2 display total alpha activities similar to those of 5C-1 and 5D-3 (Fig. 4). As mentioned previously, transuranic deposition in this area of the lagoon has probably been complex, because of the multiple sources there. The blue coral-rich layer, which contains much of the total alpha activity in these cores, may represent a relatively recent, widespread deposition. Core 5E-2 also contains a deeply buried ^{137}Cs activity peak at ca. 170 cm in coarse coral rubble (Fig. 4) and appears to have graded bedding suggestive of a large slump (Fig. 3). The stratigraphy of this core below about 50 cm probably records the cratering effects of either event Magnolia, Butternut or Rose (Fig. 2).

The distribution of radioactivity in these cores suggests that the atoll radionuclide inventory cannot be modelled simply. Previous estimates of the Enewetak Atoll radionuclide inventory identified the lagoon sediments as the largest reservoir but relied on samples within the topmost 20 cm of the sediment column (U.S.A.E.C., 1973; Noshkin, 1980). We consider these estimates to be certainly minimum values, from the data summarized in Table 2 and in Figure 4. Our samples are from a small portion of the lagoon where burial of radionuclides may only be associated with cratering of nearby barge shots, but it is these areas where the levels of contamination are greatest (U.S.A.E.C., 1973). For example, from Table 2 it is evident that the surface sediments off Runit contain an average of about 10 times more ^{60}Co and $^{239+240}Pu$ than pre-cleanup Runit soil. The ^{60}Co and $^{239+240}Pu$ activities buried within the most contaminated lagoon sediments sampled reach levels that are on average 3–10 times those of the surface.

Callianassid bioturbation has implications for both the atoll radionuclide inventory and for the mobilization of this inventory in the sediments and bottom waters of the lagoon. Burial of fallout radionuclides by the bioturbation of unspecified benthic burrowing organisms is often invoked to explain the vertical distribution of these radionuclides in the topmost 10–30 cm of marine sediments (Peng et al., 1979; Livingston and Bowen, 1979; Santschi et al., 1983), and the vigor and scale of burrowing activity has become more widely recognized (Pemberton et al., 1976; Weaver and Schultheiss, 1983; Suchanek, 1983; Suchanek and Colin, this volume; Suchanek et al., this volume). Callianassids are found at all water depths within the lagoon, and the number of large (>5 cm diameter)

mounds increases with depth from 1 per m^2 to 2.5 per m^2 below 30 m (Colin et al., this volume). Therefore, a significant portion of the initial fallout deposition to the entire lagoon sediment surface may be mixed to depths of at least 1.5 m by callianassid activity. Such deep mixing would add to the underestimation of lagoon sediment radionuclide inventories based on surface values.

Noshkin (1980) calculated that 50% of the present inventory of $^{239+240}$Pu in Enewetak lagoon sediments will be remobilized in solution and discharged to the North Equatorial Pacific over the next 250 years. These calculations are based on diffusion of $^{239+240}$Pu from the sediment surface and are in reasonable agreement with measurements of dissolved $^{239+240}$Pu in the lagoon water (Noshkin, 1980). Our results indicate that the present $^{239+240}$Pu inventory is much larger than the 249 and 1,185 Ci estimated to sediment depths of 2.5 and 16 cm by Noshkin (1980), and therefore it will take considerably longer than 250 years for 50% of the inventory to dissipate. On the other hand, the burrowing, sorting, and water and particulate pumping of callianassids combine to provide an effective means to cycle $^{239+240}$Pu and other radionuclides to the sediment–water interface where diffusion into the overlying water column would be enhanced. Further work will be needed to assess accurately the extent of the lagoon radionuclide inventory and to quantify the various effects of callianassid bioturbation on sediment and radionuclide remobilization within the lagoon.

Conclusions

Despite extensive radiological cleanup of the Enewetak Atoll islands, the sediments of the lagoon floor continue to be the largest repository of fallout radionuclides of the atoll. The long-lived radionuclides contained in these sediments are potentially able to enter into aquatic food chains and into uncontaminated areas of the atoll and surrounding ocean. It is therefore important to know the size of the radionuclide inventory and the mechanisms and rates of sediment and radionuclide distribution within the lagoon.

Our initial work has discovered that: (1) the radionuclide inventory is not confined to the surface sediments of the lagoon, as previously assumed, but is distributed within the sediment to depths of at least 2 m, the extent of our longest core; (2) the burrowing activities of callianassid ghost shrimp (Crustacea: Thalassinidea) are evident at the sediment surface throughout the sampling area and at depth in the two most heavily contaminated cores collected; and (3) the burrowing activities of these organisms facilitate the release of radionuclides buried within the sediments. Callianassid bioturbation has probably also complicated the initial surface fallout deposition to the entire lagoon floor by sediment mixing and burial to depths of at least 1.5 m.

The sediments investigated are from an area of the lagoon that was heavily contaminated by several barge detonations and events on Runit. Six of the 11 cores studied show elevated radionuclide concentrations at depth, but only the two most heavily contaminated cores display elevated concentrations which correlate with an iron-rich, predominately fine-grained (<38 μm) carbonate layer that is probably blast-pulverized reef and sediments from a nearby barge event. Over 90% of the radioactivity in this layer resides in the iron-rich, noncarbonate residue. The residue contains magnetite from vaporized barge condensation and fallout and pyrite from postdepositional alteration of the magnetite under anoxic conditions.

Subsequent burrowing into this layer by callianassids has displaced radioactive sediment and introduced less-radioactive, coarser-grained sediment. Burrowing

activities may also have introduced oxygenated porewaters to react with pyrite and magnetite, forming amorphous ferric oxides. This oxidation is proposed to release relatively soluble radionuclides such as ^{137}Cs for porewater diffusion and advection by callianassid pumping. Relatively insoluble radionuclides such as ^{60}Co and the transuranics are probably quickly reabsorbed by the ferric oxides. Although a small portion of these radionuclides may be solubilized, most are probably mobilized during callianassid burrowing, sorting and particulate pumping.

ACKNOWLEDGMENTS

We thank T. Kerby of the Hawaii Undersea Research Laboratory for technical assistance in the field and S. Wickramaratne for assistance in the laboratory. This study was supported by the U.S. Department of Energy under contract No. DE-AT03-81EV10699 (McMurtry) and contract No. DE-AC08-76EV00703 for operation of the Mid-Pacific Research Laboratory. Hawaii Institute of Geophysics Contribution No. 1678.

LITERATURE CITED

Adams, C. E., N. H. Farlow and W. R. Schell. 1960. The composition, structures and origin of radioactive fall-out particles. Geochim. Cosmochim. Acta 18: 42–56.

Alberts, J. J. and K. A. Orlandini. 1981. Laboratory and field studies of the relative mobility of $^{239+240}Pu$ and ^{241}Am from lake sediments under oxic and anoxic conditions. Geochim. Cosmochim. Acta 45: 1931–1940.

Andersen, M. E. and J. D. Macdougall. 1977. Accumulation rates of manganese nodules and sediments: an alpha track method. Geophys. Res. Lett. 4: 351–353.

Berner, R. A. 1970. Sedimentary pyrite formation. Am. J. Sci. 268: 1–23.

Bliss, W., compiler. 1982. Enewetak fact book. U.S. Dept. of Energy. Nevada Operations Office, Las Vegas. 218 pp.

Buddemeier, R. W., A. H. Biermann and C. Gatrousis. 1978. Alpha-sensitive cellulose nitrate track detectors: applications to the study of environmental contamination. Lawrence Livermore Laboratory Preprint UCRL-80679. 18 pp.

Carpenter, R. and T. M. Beasley. 1981. Plutonium and americium in anoxic marine sediments: evidence against remobilization. Geochim. Cosmochim. Acta 45: 1917–1930.

Colin, P. L., T. H. Suchanek and G. M. McMurtry. 1986. Water pumping and particulate resuspension by callianassids (Crustacea: Thalassinidea) at Enewetak and Bikini Atolls, Marshall Islands. Bull. Mar. Sci. 38: 19–24.

Davis, J. J. and R. F. Foster. 1958. Bioaccumulation of radioisotopes through aquatic food chains. Ecology 39: 530–535.

Defense Nuclear Agency. 1981. The radiological cleanup of Enewetak Atoll. Washington, D.C. 700 pp.

Emery, K. O., J. I. Tracey, Jr. and H. S. Ladd. 1954. Geology of Bikini and nearby atolls: part 1, geology. Geol. Survey Prof. Paper 260-A. 265 pp.

Fankhauser, B. L. 1976. Thermoluminescence dating applied to Hawaiian basalts. M.S. Thesis, Univ. Hawaii, Honolulu. 188 pp.

Fisher, D. E. 1977a. Fission/alpha analysis of the U, Th families. Nature 265: 227–229.

———. 1977b. f/α particle track analysis: a new geologic technique for the measurement of uranium, thorium, and isotopic disequilibria. J. Radioanal. Chem. 38: 477–490.

Gudiksen, P. H. and O. D. T. Lynch, Jr. 1975. Radioactivity levels in Enewetak soil. Health Physics 29: 17–25.

Jackson, M. L. 1974. Soil chemical analysis: advanced course, 2nd ed. Pub. by the author, Univ. Wisconsin, Madison. 895 pp.

Knutson, D. W., R. W. Buddemeier and S. V. Smith. 1972. Coral chronometers: seasonal growth bands in reef coral. Science 177: 270–272.

Livingston, H. D. and V. T. Bowen. 1979. Pu and ^{137}Cs in coastal sediments. Earth Planet. Sci. Lett. 43: 29–45.

McMurtry, G. M. 1979. Rates of sediment accumulation and their bearing on metallogenesis on the Nazca plate, southeast Pacific. Ph.D. Dissertation, Univ. Hawaii, Honolulu. 232 pp.

———, H. H. Veeh and C. Moser. 1981. Sediment accumulation rate patterns on the northwest Nazca plate. Geol. Soc. Am. Mem. 154: 211–249.

———, R. C. Schneider, P. L. Colin, R. W. Buddemeier and T. H. Suchanek. 1985. Redistribution

of fallout radionuclides in Enewetak lagoon sediments by callianassid bioturbation. Nature 313: 674–677.

Noshkin, V. E. 1980. Transuranium radionuclides in components of the benthic environment of Enewetak Atoll. Pages 578–601 *in* W. C. Hanson, ed. Transuranic elements in the environment. U.S. Dept. of Energy, Washington, D.C.

Pemberton, G. S., M. J. Risk and D. E. Buckley. 1976. Supershrimp: deep bioturbation in the Strait of Canso, Nova Scotia. Science 192: 790–791.

Peng, T.-H., W. S. Broecker and W. H. Berger. 1979. Rates of benthic mixing in deep-sea sediment as determined by radioactive tracers. Quaternary Res. 11: 141–149.

Ristvet, B. L. 1978. Geologic and geophysical investigations of the Enewetak nuclear craters. AFWL-TR-77-242. Air Force Weapons Lab, Air Force Systems Command, Kirtland AFB, New Mexico. 298 pp.

Rybach, L. 1971. Gamma-ray spectrometry for simultaneous U, Th and K determinations. Pages 301–305 *in* R. E. Wainerdi and E. A. Uken, eds. Modern methods of geochemical analysis. Plenum Press, New York.

Santschi, P. H., Y.-H. Li, D. M. Adler, M. Amdurer, J. Bell and U. P. Nyffeler. 1983. The relative mobility of natural (Th, Pb and Po) and fallout (Pu, Am, Cs) radionuclides in the coastal marine environment: results from model ecosystems (MERL) and Narragansett Bay. Geochim. Cosmochim. Acta 47: 201–210.

Suchanek, T. H. 1983. Control of seagrass communities and sediment distribution by *Callianassa* (Crustacea, Thalassinidea) bioturbation. J. Mar. Res. 41: 281–298.

——— and P. L. Colin. 1986. Rates and effects of bioturbation by invertebrates and fishes at Enewetak and Bikini Atolls. Bull. Mar. Sci. 38: 25–34.

———, ———, G. M. McMurtry and C. S. Suchanek. 1986. Bioturbation and redistribution of sediment radionuclides in Enewetak Atoll Lagoon by callianassid shrimp: biological aspects. Bull. Mar. Sci. 38: 144–154.

U.S. Atomic Energy Commission. 1973. Enewetak radiological survey. NVO-140, Vol. 1. Nevada Operations Office, Las Vegas. 736 pp.

U.S. Department of Energy. 1982. Enewetak radiological support project. NVO-213. Final report. Nevada Operations Office, Las Vegas. 349 pp.

Weaver, P. P. E. and P. J. Schultheiss. 1983. Vertical open burrows in deep-sea sediments 2 m in length. Nature 301: 329–331.

DATE ACCEPTED: August 9, 1985.

ADDRESSES: *(G.M.M. and R.C.S.) Hawaii Institute of Geophysics, University of Hawaii, Honolulu, Hawaii 96822; (P.L.C.) Motupore Island Research Department, University of Papua New Guinea, Box 320, University, Papua New Guinea; (R.W.B.) Lawrence Livermore Laboratory, University of California, Livermore, California 94550; (T.H.S.) Division of Environmental Studies, University of California, Davis, California 95616.*